

A Revised Physical Theory for Adsorption of Metal Complexes at Oxide Surfaces

KRISHNA B. AGASHE AND JOHN R. REGALBUTO¹

Chemical Engineering Department, University of Illinois at Chicago, Chicago, Illinois 60607

Received July 25, 1994; accepted July 22, 1996

The electric double-layer model of physical adsorption originally proposed by James and Healy in the early seventies (1–3) has largely been abandoned in favor of more complex triple-layer chemical adsorption models. Two refinements have been made to the original simpler double-layer model and results for the simulation of metal ion adsorption over silica, iron(III) oxide, chromium(III) oxide, and alumina are presented here. With a more accurate (non-Nernstian) description of surface potential (25, 26), and the more accurate solvation free energy term of Levine (8), good fits to the data are obtained with smaller or no adjustable “chemical” interaction terms. The interpretation of the revised model is directly contrary to the original double-layer model in that multivalent, unhydrolyzed ions are now predicted to adsorb preferentially to univalent hydrolysis products. This interpretation coincides with the results of more recent triple-layer models, indicating preferential adsorption of multivalent complexes. However, the revised physical adsorption model suggests that these adsorption phenomenon are usually physical (electrostatic) in nature and not chemical. © 1997 Academic Press

INTRODUCTION

One of the earliest models for adsorption of charged metal complexes from aqueous solution onto oxide surfaces was that of James and Healy (1–3), which was based on a predominantly physical interaction. This model incorporated an electric double layer in which the oxide surface potential was described by the Nernst equation. Adsorption free energy terms accounted for coulombic interaction (usually an attractive term) and solvation energy (a repulsive term). A main drawback of this model is often the necessity of a relatively large adjustable “chemical” free energy term. For example, in the original publication (3) to fit the adsorption of Co complexes over SiO₂, coulombic and solvation free energies were calculated at high pH to be –19 and 11 KJ/mol, respectively, while the “chemical” interaction term

took on the magnitude of –27 KJ/mol. The chemical interaction term can be made so overwhelmingly large that adsorption of cations over positively charged surfaces can be fitted with the James and Healy model (4–7).

Various formulations of chemical adsorption models, in particular “triple layer models” or TLMs (8–10), have largely replaced the physical adsorption model. In these models the “repulsion” is due to singly valent counterions such as Cl[–] or Na⁺ which bind to the protonated or deprotonated hydroxyl groups, so diminishing the potential experienced by other adsorbing ionic complexes. In the older TLMs the univalent counterions experience a higher potential than do multivalent ionic complexes, which argues against a predominantly electrostatic adsorption mechanism. Similarly, in James and Healy’s model univalent hydrolysis products such as Co(OH)⁺¹ and Fe(OH)₂⁺¹ were postulated to adsorb preferentially to the multivalent metal cations Co⁺² and Fe⁺³ (3), due to the domination of the solvation over the coulombic free energy term. Newer surface complexation models (11–21), however, predict that multivalent ions can be adsorbed in preference to univalent or lower charged ions. These predictions are based on the best fit of the surface complexation model to the experimental data.

Revisions of the solvation energy component have recently been made for physical surface complexation (22) as well as ion exchange (23) models. In fact, a more rigorous derivation for this term was provided by Levine (8) early on, as noted by Fuerstenau and Osseao-Asare (24), but to the authors’ knowledge it has never been evaluated. In the present work this term has been incorporated into James and Healy’s original model. An additional refinement is that surface potential has been calculated with a more realistic non-Nernstian treatment of the oxide surface (25, 26). Good agreement to experimental data for adsorption over silica above the pzc, Fe(III) and Cr(III) oxides, and alumina, above and below the pzc, is achieved with smaller values of the “chemical interaction term,” and in some cases even without this term. A most notable result is that the revised model contradicts the original interpretation that univalent hydrolysis products adsorb preferentially to multivalent unhydrolyzed ions over silica above the pzc. According to the

¹ To whom correspondence should be addressed.

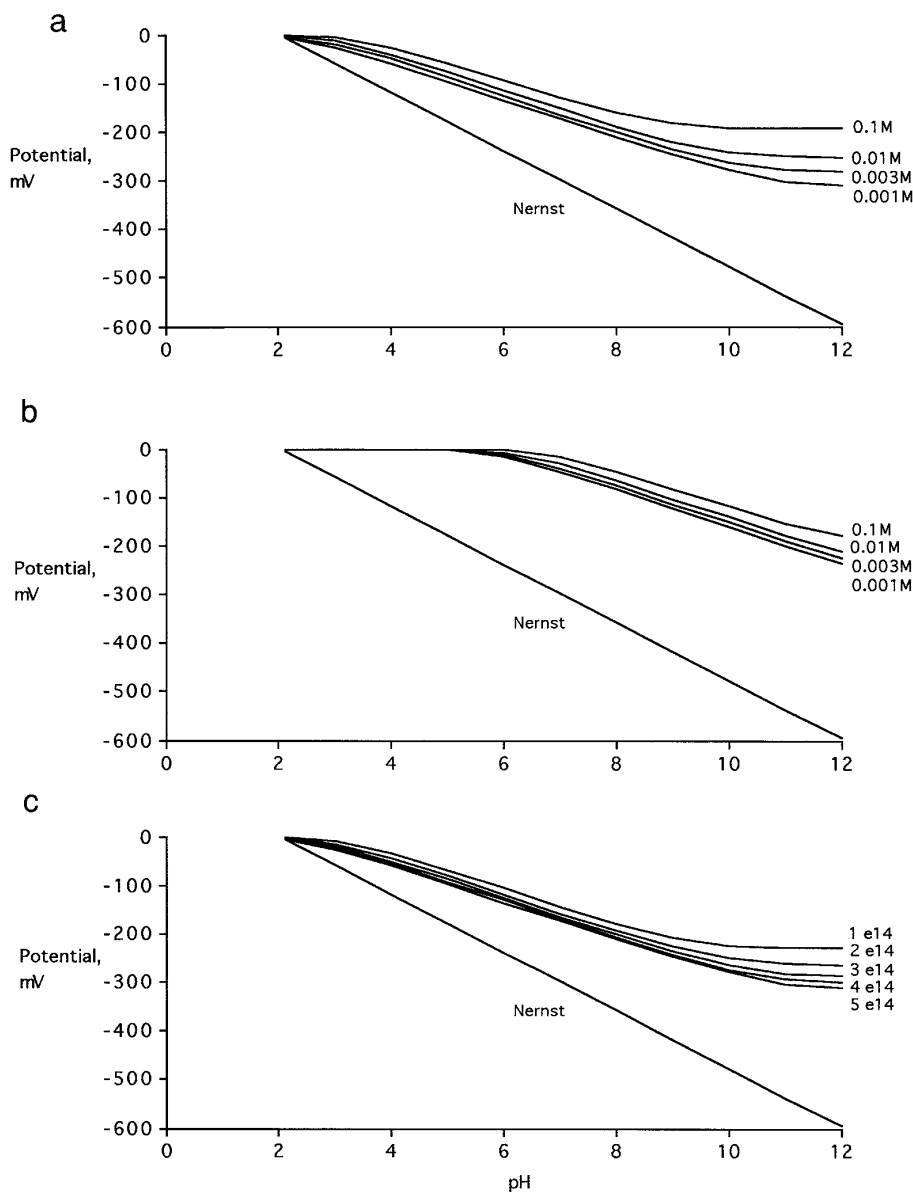


FIG. 1. Variation of potential from Nernstian as a function of (a) ionic strength at $\Delta pK = 5.2$ and $N_s = 5e14$ sites/cm², (b) ionic strength at $\Delta pK = 8.5$ and $N_s = 5e14$ sites/cm², (c) surface site density (N_s sites/cm²) at constant $\Delta pK = 5.2$.

present calculations the coulombic term dominates all others. There may be a good number of systems in which the mechanism of adsorption is chiefly physical and not chemical.

THEORY

A Langmuir adsorption isotherm is employed, and the maximum adsorption density Γ_{mi} (mole/area) is based on a steric close-packed layer of adsorbates retaining one hydration sheath:

$$\Gamma_T \left(\frac{\text{mole}}{\text{area}} \right) = \sum_i \Gamma_i = \frac{\sum_i \Gamma_{mi} K_i C_i}{1 + \sum_i K_i C_i} \quad [1]$$

The total surface covered by adsorbing species is given as a linear summation of the fraction of surface covered by individual adsorbing species,

$$\theta(\text{monolayers}) = \sum_i \theta_i = \sum_i \frac{\Gamma_i}{\Gamma_{mi}}, \quad [2]$$

where

$$\Gamma_{mi} = \left[\frac{1}{N_0 \pi (r_i + 2r_w)^2} \right] \quad [3]$$

TABLE 1
Speciation Mechanisms of Various Metal Complexes
in Undersaturated Solutions

Reaction number <i>i</i>	Mechanism	$pK_{a,i}$
Cobalt speciation mechanism		
1	$\text{Co}^{+2} + \text{H}_2\text{O} \rightleftharpoons \text{Co}(\text{OH})^+ + \text{H}^+$	9.6
2	$\text{Co}(\text{OH})^+ + \text{H}_2\text{O} \rightleftharpoons \text{Co}(\text{OH})_2^0 + \text{H}^+$	9.2
3	$\text{Co}(\text{OH})_2^0 + \text{H}_2\text{O} \rightleftharpoons \text{Co}(\text{OH})_3^- + \text{H}^+$	12.7
Calcium speciation mechanism		
1	$\text{Ca}^{+2} + \text{H}_2\text{O} \rightleftharpoons \text{Ca}(\text{OH})^+ + \text{H}^+$	12.6
Chromium speciation mechanism		
1	$\text{Cr}^{+3} + \text{H}_2\text{O} \rightleftharpoons \text{Cr}(\text{OH})^{+2} + \text{H}^+$	4.1
2	$\text{Cr}(\text{OH})^{+2} + \text{H}_2\text{O} \rightleftharpoons \text{Cr}(\text{OH})_2^+ + \text{H}^+$	5.9
3	$\text{Cr}(\text{OH})_2^+ + \text{H}_2\text{O} \rightleftharpoons \text{Cr}(\text{OH})_3^0 + \text{H}^+$	7.0
Iron speciation mechanism		
1	$\text{Fe}^{+3} + \text{H}_2\text{O} \rightleftharpoons \text{Fe}(\text{OH})^{+2} + \text{H}^+$	2.2
2	$\text{Fe}(\text{OH})^{+2} + \text{H}_2\text{O} \rightleftharpoons \text{Fe}(\text{OH})_2^+ + \text{H}^+$	4.0
3	$\text{Fe}(\text{OH})_2^+ + \text{H}_2\text{O} \rightleftharpoons \text{Fe}(\text{OH})_3^0 + \text{H}^+$	5.1
4	$\text{Fe}(\text{OH})_3^0 + \text{H}_2\text{O} \rightleftharpoons \text{Fe}(\text{OH})_4^- + \text{H}^+$	11.9
Nickel speciation mechanism		
1	$\text{Ni}^{+2} + \text{H}_2\text{O} \rightleftharpoons \text{Ni}(\text{OH})^+ + \text{H}^+$	9.86
2	$\text{Ni}^{+2} + 2\text{H}_2\text{O} \rightleftharpoons \text{Ni}(\text{OH})_2^0 + 2\text{H}^+$	19.00
3	$\text{Ni}^{+2} + 3\text{H}_2\text{O} \rightleftharpoons \text{Ni}(\text{OH})_3^- + 3\text{H}^+$	30.50

The steric basis for Γ_{mi} of metal cations was indicated by James and Healy (3) and has been more recently demonstrated for the adsorption of noble metal chloride anions and ammine cations over silica and alumina (27).

Adsorption equilibrium constants for species *i*,

$$K_i = \exp\left(\frac{-\Delta G_{\text{ads},i}}{RT}\right) \quad [4]$$

are calculated from an overall Gibbs free energy of adsorption, $\Delta G_{\text{ads},i}$, comprised of three terms, an attractive coulombic term, a repulsive solvation term, and what is in practice an adjustable or "chemical" free energy term (3):

$$\Delta G_{\text{ads},i} = \Delta G_{\text{coul},i} + \Delta G_{\text{solv},i} + \Delta G_{\text{chem},i} \quad [5]$$

The coulombic contribution of species *i* is given as

$$\Delta G_{\text{coul},i} = z_i F \Psi_{x,i}, \quad [6]$$

where z_i is the charge of the species, *F* the Faraday constant, and $\Psi_{x,i}$, the potential, as found from the solution of Laplace's equation. The solution of Gouy and Chapman assuming a simple electric double layer in which all species adsorb in one plane is given by (3)

$$\Psi_{x,i} = \left[\frac{2RT}{ZF} \right] \ln \left[\frac{(Y+1) + (Y-1)e^{-\kappa x_i}}{(Y+1) - (Y-1)e^{-\kappa x_i}} \right], \quad [7]$$

where

$$x_i = r_i + 2r_w(\text{m}) \quad [8]$$

and

$$Y = \exp\left(\frac{ZF\Psi_0}{2RT}\right). \quad [9]$$

The surface potential Ψ_0 will be detailed below. The Debye-Huckel reciprocal double-layer length κ is a function of ionic strength *I*:

$$\kappa = 3.31 \times 10^9 \sqrt{I} (\text{m}^{-1}), \quad I = \frac{1}{2} \sum_i z_i^2 C_i. \quad [10]$$

Typical values of $1/\kappa$ are less than the average pore radius of high surface area oxide powders; for example, at an ionic strength of $10^{-3} M$, $1/\kappa = 10.4 \text{ nm}$.

The first of two revisions of James and Healy's original computation is the treatment of surface potential (Ψ_0). The Nernst equation is not in fact a good description for the charging behavior of nonelectrode materials such as clays and inorganic oxides (25, 26, 28, 29). Healy and White have presented a number of more realistic "non-Nernstian" representations for oxide surfaces; that which is most suitable for silica is a single site model owing to its low isoelectric point (near 2) and its relative inability to attain a positive surface charge. Thus a single surface ionization constant is used to describe surface charging:

$$[\text{SiOH}]^{K'_2} [\text{SiO}^-] [\text{H}_s^+] \text{ or} \quad K'_2 = [\text{SiO}^-] [\text{H}_s^+] / [\text{SiOH}]. \quad [11]$$

The non-Nernstian model requires the simultaneous solution of three equations. First, it requires a statement of the electrical neutrality of the double layer,

$$\sigma_o + \sigma_d = 0, \quad [12]$$

where

$$\sigma_d = -(2\epsilon 10^{-3} N_o c kT / \Pi)^{1/2} \sinh(e\Psi_0 / 2kT) \quad [13]$$

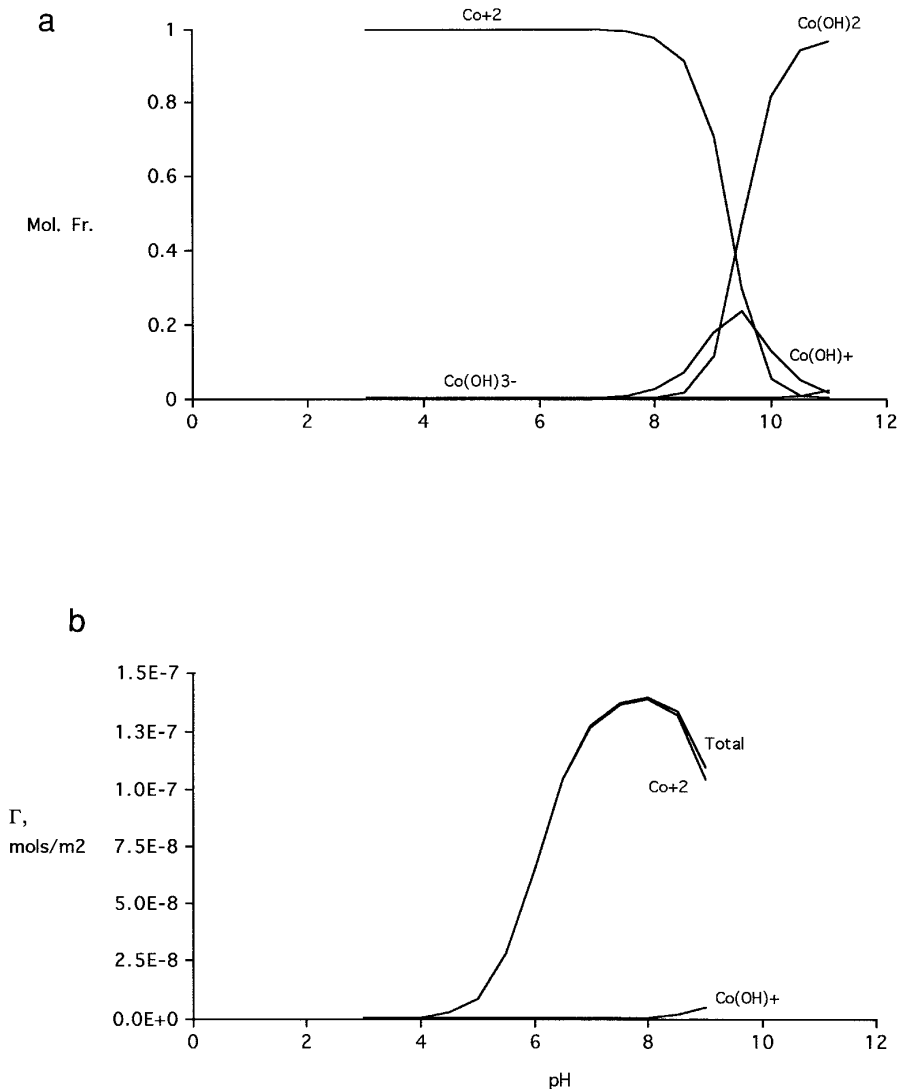


FIG. 2. (a) Variation of liquid bulk equilibrium speciation of cobalt as a function of pH of the impregnating solution. (b) Comparison of overall adsorption density with individual complex densities as a function of pH of cobalt impregnating solution for initial metal concentration of 1.2×10^{-5} and ionic strength of 0.001 mol/liter for $\Delta pK = 5.2$ and $N_s = 5 \times 10^{14}$ sites/cm².

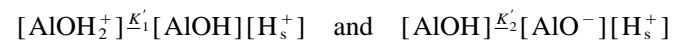
is the diffuse layer charge according to the Gouy–Chapman theory. Finally, the surface charge for single-site oxides like SiO₂, in terms of surface potential, is

$$\sigma_o = -eN_s \frac{(K'_2/H)e^{e\Psi_0/2kT}}{1 + (K'_2/H)e^{e\Psi_0/2kT}}. \quad [14]$$

Two parameters are adjustable, the total number of charged sites N_s and the difference between pK'_1 and pK'_2 ($= \Delta pK$), which equals pK'_2 for the single-site model ($pK'_1 = 0$). The ΔpK values for SiO₂ fluctuate widely depending on the source (28, 30–33), which is understandable not only in light of differing treatment conditions and methods of manufacture, but also in light

of the difficulty in measuring this value (30, 31). The two values for ΔpK chosen for this work, 5.2 and 8.5, with $N_s = 5 \times 10^{14}$ site/cm², represent the typical range of values reported in the literature.

The corresponding two-site surface charging mechanism for amphoteric oxides like Al₂O₃, which show positive charge below pzc and negative charge above the pzc, is



or

$$K'_1 = \frac{[\text{AlOH}] [\text{H}_s^+]}{[\text{AlOH}_2^+]} \quad \text{and} \quad K'_2 = \frac{[\text{AlO}^-] [\text{H}_s^+]}{[\text{AlOH}]}, \quad [15]$$

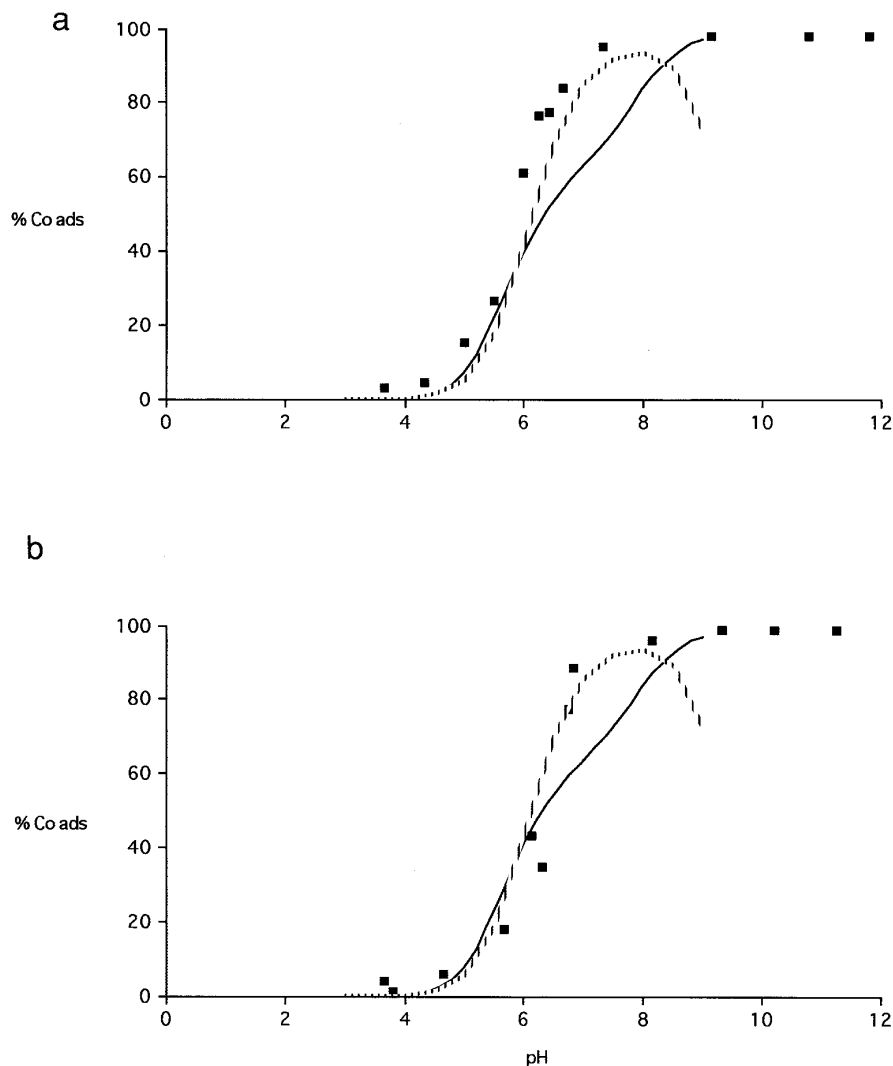


FIG. 3. (a) Comparison of experimental and RPA model uptake of cobalt on 75 m²/liter of SiO₂ at 25°C with initial metal concentration of 1.2e-6 and ionic strength of 0.001 mol/liter: (squares) experimental, (solid line) James and Healy's $\Delta G_{\text{chem},i} = -27.17$ KJ/mol, (hatched line) RPA model with $\Delta pK = 5.2$ and $N_s = 5e14$ sites/cm² $\Delta G_{\text{chem},i} = 0$ KJ/mol). (b) Comparison of experimental and RPA model uptake of cobalt on 75 m²/liter of SiO₂ at 25°C with initial metal concentration of 1.2e-5 and ionic strength of 0.001 mol/liter: (squares) experimental, (solid line) James and Healy's $\Delta G_{\text{chem},i} = -27.17$ KJ/mol, (hatched line) RPA model with $\Delta pK = 5.2$ and $N_s = 5e14$ sites/cm² $\Delta G_{\text{chem},i} = 0$ KJ/mol).

and the surface charge is

$$\sigma_o = eN_s \frac{(H/K'_1)e^{-e\Psi_0/2kT} - (K'_2/H)e^{e\Psi_0/2kT}}{1 + (H/K'_1)e^{-e\Psi_0/2kT} + (K'_2/H)e^{e\Psi_0/2kT}}. \quad [16]$$

The surface potentials calculated with the non-Nernstian model using a single-site model for SiO₂ are compared to the Nernstian equation ($\Psi_0 = [2.303RT/ZF][\text{pH}_{\text{pzc}} - \text{pH}]$) in Figs. 1a and 1b, at the two values of ΔpK and for different ionic strengths. Deviations from Nernstian behavior are always significant and are larger with the higher ΔpK value of 8.5 (Fig. 1b). The surface potential is also seen to be a moderately strong function of ionic strength. Figure 1c

shows the variation of surface potential as a function of surface site density; lower site density produces lower potential and higher site density gives high potentials.

Oxide surfaces can dramatically affect bulk liquid pH due to proton adsorption/desorption as the surface becomes protonated/deprotonated at pH values below/above its pzc (31). The two-site or amphoteric model of surface charging has been used recently in conjunction with a proton balance between the bulk liquid and surface to demonstrate that even small amounts of oxide surface exert a strong influence on liquid phase pH due to proton transfer to or from the surface (34). Thus the non-Nernstian model, besides providing a more realistic description of the surface charge, can also provide for the prediction of pH shifts due to "oxide buff-

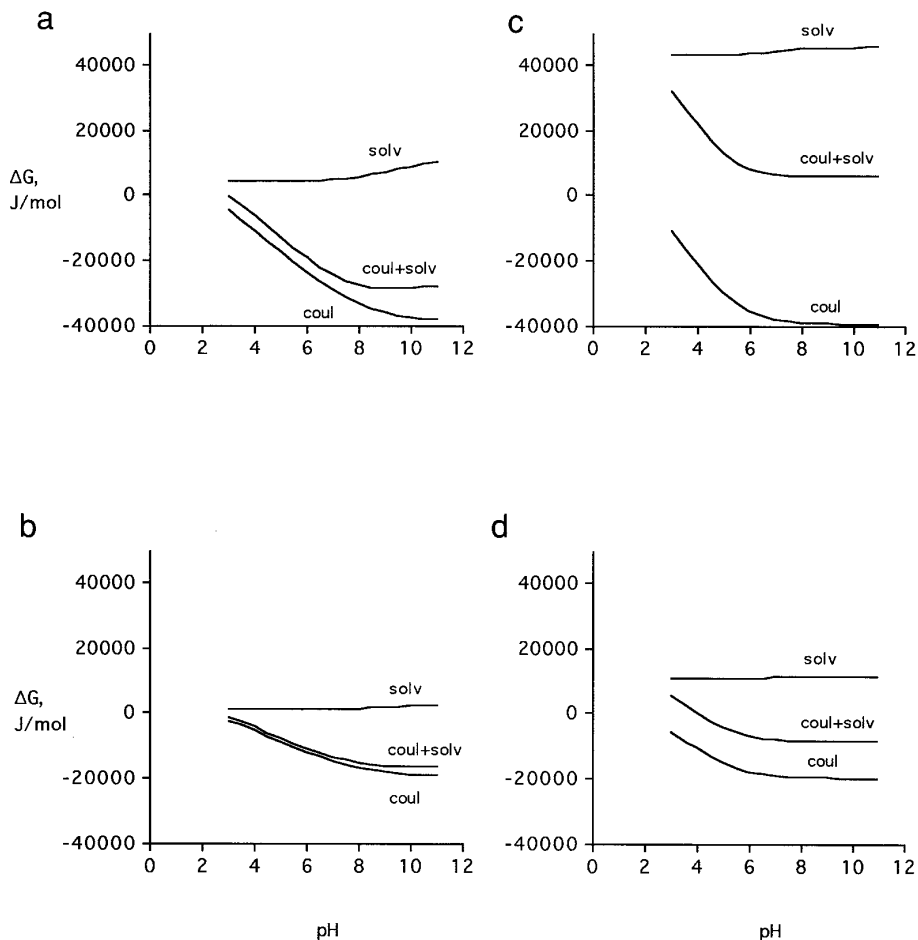


FIG. 4. (a, b) Variation of Gibbs free energy of adsorption and its components as a function of pH of cobalt impregnating solution of 1.2×10^{-5} and 1.2×10^{-6} and ionic strength 0.001 mol/liter for +2 and +1 charged complexes ($\Delta pK = 5.2$ and $N_s = 5 \times 10^{14}$ sites/cm²). (c, d) Variation of Gibbs free energy of adsorption and its components as a function of pH of cobalt impregnating solution of 1.2×10^{-5} and 1.2×10^{-6} and ionic strength 0.001 mol/liter for +2 and +1 charged complexes (James and Healy).

ering.” In most references cited herein pH shifts induced by the addition of oxide appear to have been neglected. Thus the reported pH values, presumed to be the final values, are employed in the present calculations and the proton balance and calculation of pH shifts was not included.

The second alteration of the original theory is in the solvation energy term. This term reflects the energy required to move a species from the liquid bulk to the interfacial region; the energy required to establish an electric field around an interfacial ion differs from that of the bulk solution, which is a consequence of the difference between the dielectric constants of these two regions.

A correction given by Levine (8) to the admitted overestimation of the original solvation energy term (3) is employed here. Of the three cases presented (8), that which corresponds to the double-layer model, that is, for a model in which the locus of all point charges $z_i e$ lie in one plane, is

$$\Delta G_{\text{solv},i} = \frac{1}{2} z_i e \Phi_i + \frac{(z_i e)^2}{8\pi\epsilon_0 x_i} \left(\frac{1}{\epsilon_1} - \frac{1}{\epsilon} \right), \quad [17]$$

where Φ_i is the potential at a point $r_i + 2r_w$ in the aqueous phase outside the hydration shell (8), and

$$\Phi_i = \frac{z_i e}{8\pi\epsilon_0 \epsilon_1 x_i} \left[\frac{f_1 + f_2}{\sqrt{f_1 f_2}} \tan^{-1} |f_1 f_2|^{1/2} - \ln(1 + |f_1 f_2|) \right], \quad [18]$$

where

$$f_1 = \frac{\epsilon_1 - \epsilon_p}{\epsilon_1 + \epsilon_p} \quad [19]$$

and

$$f_2 = \frac{\epsilon_1 - \epsilon}{\epsilon_1 + \epsilon}. \quad [20]$$

The interfacial dielectric constant is calculated per James and

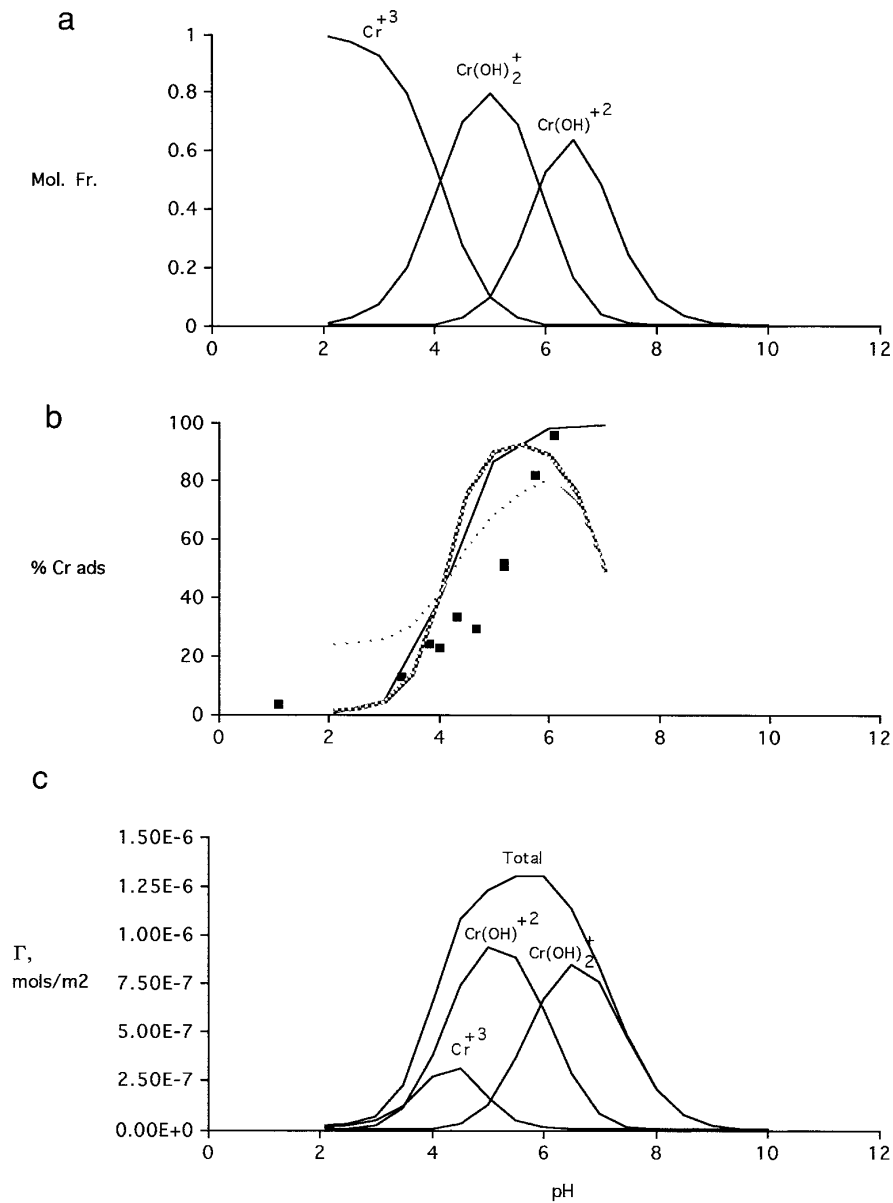


FIG. 5. (a) Variation of liquid bulk equilibrium speciation of chromium as a function of pH of the impregnating solution. (b) Comparison of experimental and RPA model uptake of chromium on 75 m²/liter of SiO₂ at 25°C with initial metal concentration of 2.0e-4 and ionic strength of 0.01 mol/liter: (squares) experimental, (solid line) James and Healy's $\Delta G_{chem,i} = -29.26$ KJ/mol, (hatched line) RPA model with $\Delta pK = 5.2$ and $N_s = 5e14$ sites/cm² $\Delta G_{chem,i} = -17$ KJ/mol, (dashed line) RPA model with $\Delta pK = 8.5$ and $N_s = 5e14$ sites/cm², $\Delta G_{chem,i} = -25.5$ KJ/mol). (c) Comparison of overall adsorption density with individual complex densities as a function of pH of chromium impregnating solution for initial metal concentration of 2.0e-4 and ionic strength of 0.01 mol/liter for $\Delta pK = 5.2$ and $N_s = 5e14$ sites/cm².

Healy (3) and is a modified form of the equation proposed by Sacher and Laidler (35), which is similar to the expression proposed by Anderson and Bockris (36), but in a much simplified form:

$$\epsilon_1 = \left(\frac{\epsilon_{bulk} - 6}{1 + (1.2 \times 10^{-17})(d\Psi/dx)_{r_w}^2} \right) + 6 \quad [21]$$

and

$$\frac{d\Psi}{dx} = -2\kappa \frac{RT}{ZF} \sinh\left(\frac{ZF\Delta\Psi_{r_w}}{2RT}\right). \quad [22]$$

The distance at which the potential gradient is calculated

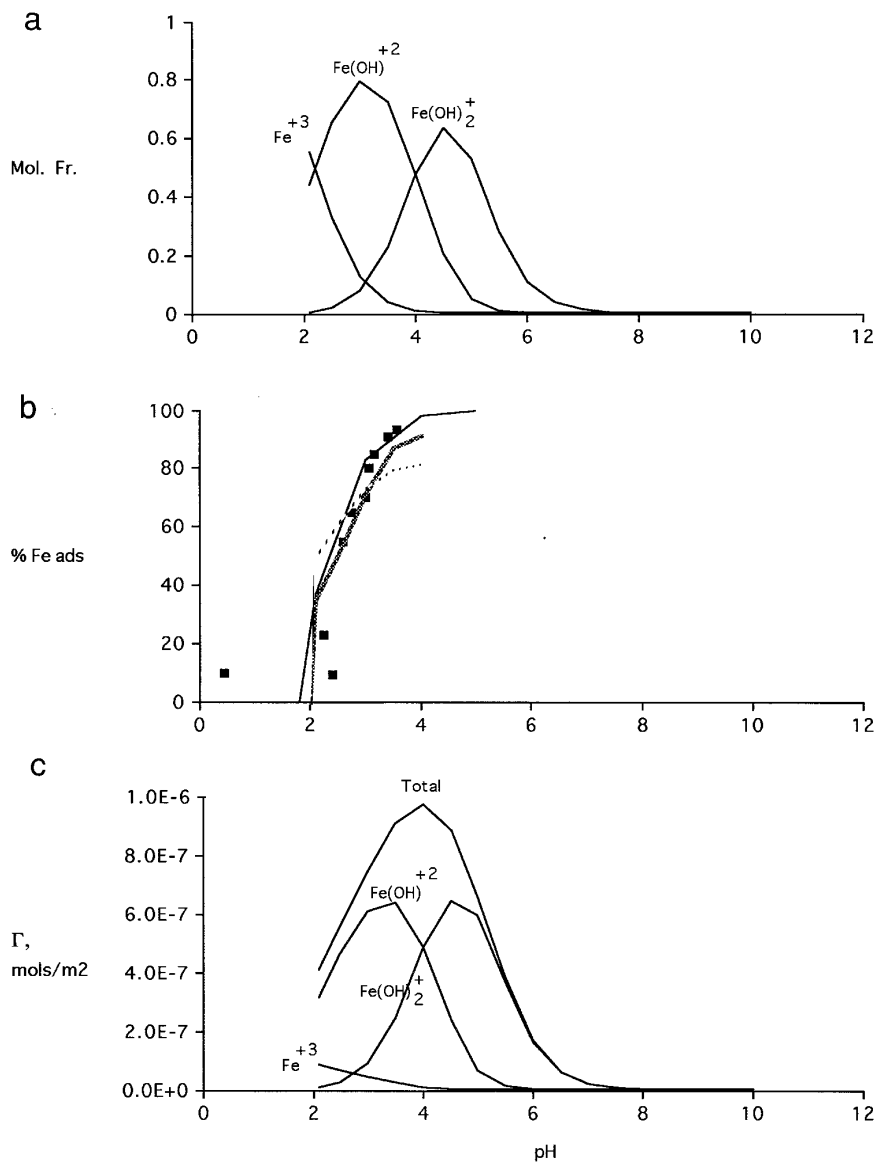


FIG. 6. (a) Variation of liquid bulk equilibrium speciation of iron as a function of pH of the impregnating solution. (b) Comparison of experimental and RPA model uptake of iron on 75 m²/liter of SiO₂ at 25°C with initial metal concentration of 1.2e-4 and ionic strength of 0.01 mol/liter: (squares) experimental, (solid line) James and Healy's $\Delta G_{\text{chem},i} = -35.53$ KJ/mol, (hatched line) RPA model with $\Delta pK = 5.2$ and $N_s = 5e14$ sites/cm² $\Delta G_{\text{chem},i} = -24.5$ KJ/mol, (dashed line) RPA model with $\Delta pK = 8.5$ and $N_s = 5e14$ sites/cm², $\Delta G_{\text{chem},i} = -27$ KJ/mol). (c) Comparison of overall adsorption density with individual complex densities as a function of pH of iron impregnating solution for initial metal concentration of 1.2e-4 and ionic strength of 0.01 mol/liter for $\Delta pK = 5.2$ and $N_s = 5e14$ sites/cm².

is a matter of some confusion in the literature. In James' Ph.D. dissertation (37), the distance r_w is employed. This value is used by Crawford *et al.* (5, 6). Fuerstenau and Osseo-Assare (24) and Theis' group (38), however, employ a value of $x = r_i + 2r_w$, as is printed in the original James and Healy manuscript (3). In fact, the James and Healy solvation term varies only by a few percentage points when the two different values are used. A careful reproduction of the ΔG_{solv} values generated by the original

model, from Fig. 8 of (3), reveals that indeed the distance of r_w was used in that work. This distinction is now vital since Levine's solvation term is a much stronger function of interfacial distance.

Levine showed that for the case of adsorption of Ba⁺², James and Healy's original term overestimates the solvation energy by a factor of about 2 when compared with the value obtained from the above term (8). As will be discussed later, the relatively small magnitude of Levine's

TABLE 2
Comparison of ΔG_{chem} Terms

Species	James and Healy's ΔG_{chem} (KJ/mol)	RPA model	
		ΔpK	ΔG_{chem} (KJ/mol)
Fe+3, Fe+2, Fe+ $r_{\text{Fe}} = 0.64$ (Å)	-35.5	5.2 8.5	-24.5 -27.0
Cr+3, CR+2, Cr+1 $r_{\text{Cr}} = 0.69$ (Å)	-29.3	5.2 8.5	-17.0 -25.5
Ni+2, Ni+1 $r_{\text{Ni}} = 0.79$ (Å)	-27.4	5.2 8.5	-10.0 -14.5
Ca+2, Ca+1 $r_{\text{Ca}} = 0.99$ (Å)	-29.3	5.2 8.5	-5.0 -5.0
Co+2, Co+1 1.2E-4M $r_{\text{Co}} = 0.78$ (Å)	-27.2	5.2 8.5	0.0 -15.0
Co+2, Co+1 1.2E-5M, 1.2E-6M $r_{\text{Co}} = 0.78$ (Å)	-27.2	5.2 8.5	0.0 -15.0

term is the source of the vastly different phenomenological interpretation of the revised model; the coulombic term becomes dominant.

Experiments to be simulated are at constant ionic strength, in which case the adsorption equilibrium constants are truly constant. The solutions considered are undersaturated so that the liquid-phase mole fractions are independent of total metal concentration. The liquid-phase speciation of the metal cations is found from known hydrolysis constants, listed in Table 1. The equilibrium liquid-phase concentration of each species is found from a mole balance on each species,

$$C_i = C_{i,\text{initial}} - C_{i,\text{adsorbed}}, \quad [23]$$

where the amount adsorbed $C_{i,\text{adsorbed}}$ is calculated as

$$C_{i,\text{ads}} = \frac{m_{\text{OX}} S_{\text{OX}}}{V_L} \Gamma_i = \frac{m_{\text{OX}} S_{\text{OX}}}{V_L} \left(\frac{\Gamma_{mi} K_i C_i}{1 + \sum_i K_i C_i} \right). \quad [24]$$

If one species is predominantly adsorbed, at constant ionic strength, the mole balance becomes a quadratic function of C_i of the dominant species. The surface potential and adsorption uptake can be calculated sequentially in the manner of Dzombak and Morel (11) using common equation solver and spreadsheet packages.

In some instances the revised model actually possesses two adjustable parameters, ΔpK and ΔG_{chem} , instead of the one (ΔG_{chem}) in the original model. The value of ΔpK is a measurable quantity (although not accurately so (30–31)) and in principle can be measured independently. To simulate

the alumina data of reference (39), the reported value of ΔpK was used with no adjustment. However, for adsorption results over SiO_2 (1–3, 37), ΔpK was not available. The approach was to attempt a good fit by adjusting only ΔpK with $\Delta G_{\text{chem}} = 0$. (At any value of ΔpK , a more realistic description of the surface than the Nernst equation should result.) If good agreement was still not achieved, the ΔG_{chem} term was employed.

RESULTS AND DISCUSSION

The liquid-phase speciation of cobalt and the adsorption density of cobalt species are shown in Figs. 2a and 2b, while comparisons of the revised double layer model to James and Healy's data and their model are made in Fig. 3 for the two undersaturated concentrations they reported (1). The agreement of the revised model is somewhat better in the pH range up to 8. The revised model predicts a dropoff in adsorption past a pH of 8, due to the prevalence of the zero-valent second hydrolysis product $\text{Co}(\text{OH})_2$ in solution. James and Healy's original model exhibits this dropoff past a pH of 9 due to the large magnitude of the ΔG_{chem} parameter. However, in their original manuscript, as here, calculations were not extended beyond a pH of 9 due to another physical phenomenon. James and Healy unambiguously demonstrated with zeta potentiometry that this phenomenon was associated with a negative-to-positive charge reversal (2), implying that Co was adsorbed in amounts beyond one monolayer. They attributed this behavior to surface precipitation, which would occur at a pH somewhat lower than that in the bulk solution. Neither their original model nor the present revised model include a consideration of surface precipitation.

The revised model incorporates more accurate surface potential and solvation free energy calculations and provides a good fit to the data with a fitted value of the surface potential within a commonly cited range. The interpretation of adsorption phenomenon, however, is completely at odds with the original model. Looking back to Fig. 2b, it is seen that the divalent Co^{+2} cation is the preferentially adsorbed species. In the original model, the first hydrolysis product was thought to be the predominantly adsorbed species. The difference in interpretation can be seen in the individual free energies for the +2 and +1 species, shown in Fig. 4. The solvation, coulombic, and total free energies for the +2 and +1 cobalt species, for Levine's solvation free energy term, are shown in Figs. 4a and 4b, while the James and Healy counterparts are shown in Figs. 4c and 4d. Of immediate note is that the solvation free energies using Levine's calculations are much smaller than those of James and Healy's term. In fact, in James and Healy's original model, the solvation energy dominated the total free energy of adsorption and was so high for the +2 species that the overall free energy for this species was positive. With the much smaller

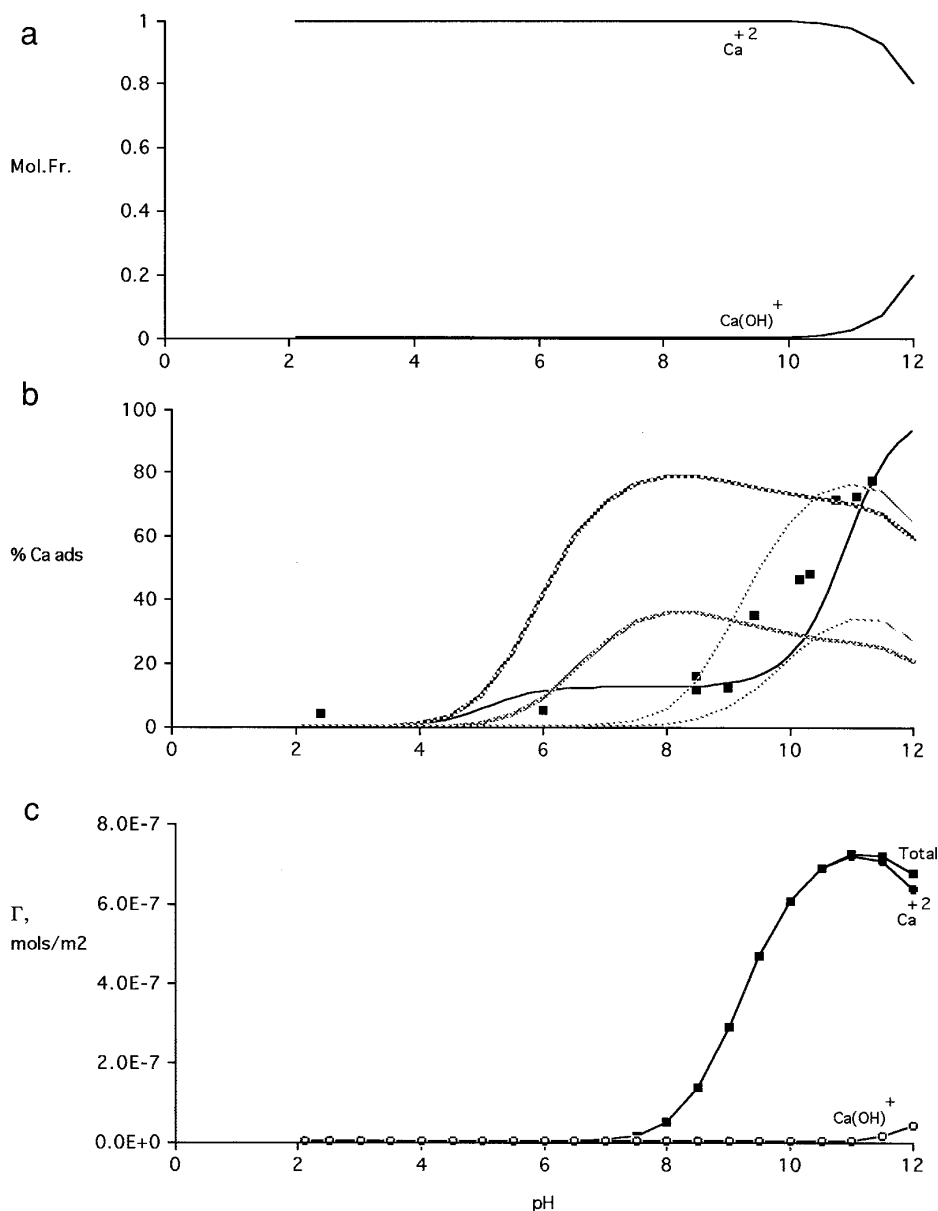


FIG. 7. (a) Variation of liquid bulk equilibrium speciation of calcium as a function of pH of the impregnating solution. (b) Comparison of experimental and RPA model uptake of calcium on 75 m²/liter of SiO₂ at 25°C with initial metal concentration of 1.4e-4 and ionic strength of 0.01 mol/liter: (squares) experimental, (solid line) James and Healy's $\Delta G_{\text{chem},i} = -29.26$ KJ/mol; (upper hatched line) RPA model with $\Delta pK = 5.2$ and $N_s = 5e14$ sites/cm², $\Delta G_{\text{chem},i} = -5$ KJ/mol; (lower hatched line) RPA model with $\Delta pK = 5.2$ and $N_s = 5e14$ sites/cm², $\Delta G_{\text{chem},i} = 0$ KJ/mol; (upper dashed line) RPA model with $\Delta pK = 8.5$ and $N_s = 5e14$ sites/cm², $\Delta G_{\text{chem},i} = -5$ KJ/mol; (lower dashed line) RPA model with $\Delta pK = 8.5$ and $N_s = 5e14$ sites/cm², $\Delta G_{\text{chem},i} = 0$ KJ/mol). (c) Comparison of overall adsorption density with individual complex densities as a function of pH of calcium impregnating solution for initial metal concentration of 1.4e-4 and ionic strength of 0.01 mol/liter for $\Delta pK = 8.5$ and $N_s = 5e14$ sites/cm².

solvation energy of Levine, it is the coulombic term that dominates. Thus, the revised double-layer model offers a principally "electrostatic" interpretation of the adsorption phenomenon over silica.

With the revised model, the +2 adsorbed Co species (Fig. 2b) mirrors the predominance of the +2 species in the liquid phase (Fig. 2a), at least when surface potential has developed enough for adsorption to occur strongly. In the original

model, the +1 species was predicted to be the predominant adsorbing species even though its concentration was orders of magnitude less than that of the +2 species in the liquid phase.

The liquid phase speciation, adsorption density, and comparison to experimental data for two trivalent cations, Cr and Fe, are shown in Figs. 5 and 6, respectively. Reasonable fits of the data were obtained with the same ΔpK value as

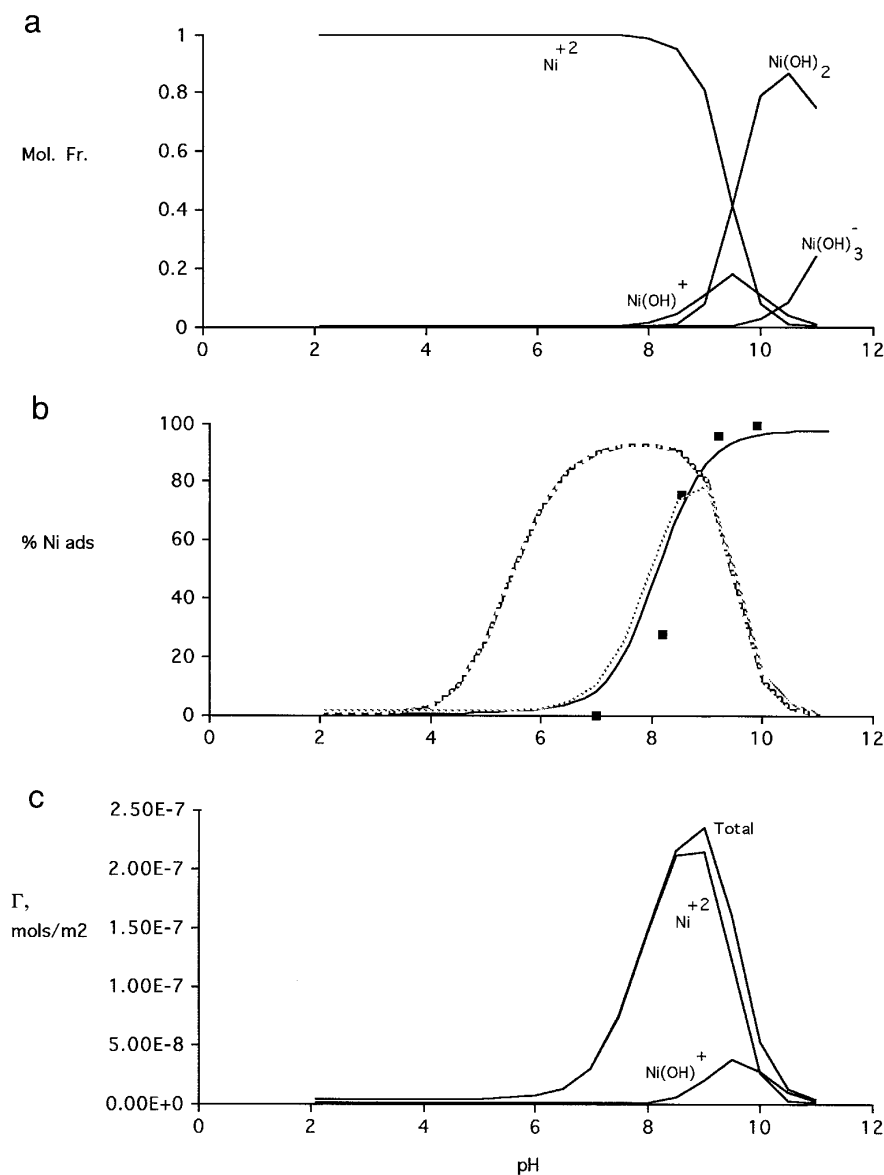


FIG. 8. (a) Variation of liquid bulk equilibrium speciation of nickel as a function of pH of the impregnating solution. (b) Comparison of experimental and RPA model uptake of nickel on 50 m²/liter of SiO₂ at 25°C with initial metal concentration of 1.7e-5 and ionic strength of 0.01 mol/liter: (squares) experimental, (solid line) Thais and Richter's $\Delta G_{\text{chem},i} = -27.17$ KJ/mol, (hatched line) RPA model with $\Delta pK = 5.2$ and $N_s = 5e14$ sites/cm² $\Delta G_{\text{chem},i} = -10$ KJ/mol, (dashed line) RPA model with $\Delta pK = 8.5$ and $N_s = 5e14$ sites/cm², $\Delta G_{\text{chem},i} = -14.5$ KJ/mol). (c) Comparison of overall adsorption density with individual complex densities as a function of pH of nickel impregnating solution for initial metal concentration of 1.7e-5 and ionic strength of 0.01 mol/liter for $\Delta pK = 8.5$ and $N_s = 5e14$ sites/cm².

used previously, 5.2, but ΔG_{chem} terms had to be added in order to match the high level of uptake. The values of ΔG_{chem} used in the revised model, as well as those originally employed by James and Healy, are shown for all simulations in Table 2. The values used in the present model for Cr and Fe, -17 and -24.5 KJ/mol, are considerably smaller in magnitude than the corresponding terms of the original model, -29 and -35.5 KJ/mol, respectively. Although the revised model has an added adjustable parameter in ΔpK , the non-Nernstian treatment provides a more realistic de-

scription of the oxide surface potential. The smaller ΔG_{chem} values of the revised model may well reflect a more realistic description of the entire adsorption process.

According to the revised model, the coulombic free energy term also dominates for the trivalent species, and while the triply valent cations possess the most negative free energies of adsorption, their adsorption densities are low (Figs. 5c and 6c) due to their low concentrations. In both of these cases, the adsorption density of the individual surface species again mirrors that of the liquid-phase species.

TABLE 3
Individual ΔG Values at pH 7.0

	Original James and Healy model					RPA model			
	ΔG_{coul} (KJ/mol)	ΔG_{solv} (KJ/mol)	ΔG_{chem} (KJ/mol)	ΔG_{ads} (KJ/mol)		ΔG_{coul} (KJ/mol)	ΔG_{solv} (KJ/mol)	ΔG_{chem} (KJ/mol)	ΔG_{ads} (KJ/mol)
Ni +2	23.1	22.6	-44.0	1.71	$\Delta pK = 5$	19.7	4.22	-35.0	-11.1
					$\Delta pK = 7$	13.6	4.19	-30.0	-12.2
Ni + 1	11.5	5.66	-44.0	-26.8	$\Delta pK = 5$	9.84	1.06	-35.0	-24.1
					$\Delta pK = 7$	6.81	1.05	-30.0	-22.2
Zn +2	13.0	11.5	-45.0	-20.5	$\Delta pK = 5$	11.5	3.51	-35.0	-19.9
					$\Delta pK = 7$	6.91	3.51	-27.0	-16.6
Zn +1	6.52	2.86	-45.0	-35.6	$\Delta pK = 5$	5.75	0.879	-35.0	-28.4
					$\Delta pK = 7$	3.46	0.878	-27.0	-22.7
Cr +3	19.6	26.2	-50.0	-4.29	$\Delta pK = 5$	17.3	8.02	-50.0	-24.7
					$\Delta pK = 7$	10.4	8.01	-40.0	-21.6
Cr +2	13.0	11.6	-50.0	-25.3	$\Delta pK = 5$	11.5	3.57	-50.0	-34.9
					$\Delta pK = 7$	6.92	3.56	-40.0	-29.5
Cr +1	6.52	2.91	-50.0	-40.6	$\Delta pK = 5$	5.76	0.891	-50.0	-43.4
					$\Delta pK = 7$	3.46	0.890	-40.0	-35.6
Pb +2	10.7	12.3	-32.0	-9.03	$\Delta pK = 5$	7.92	3.44	-30.0	-18.6
					$\Delta pK = 7$	3.41	3.42	-30.0	-23.1
Pb +1	5.35	3.07	-32.0	-23.6	$\Delta pK = 5$	3.96	0.859	-30.0	-25.2
					$\Delta pK = 7$	1.71	0.855	-30.0	-27.4

Finally, simulations for two other divalent cations, Ni and Ca, are shown in Figs. 7 and 8. For both cations, the previous ΔpK value of 5.2 resulted in too high a surface potential and predicted adsorption to occur much sooner than observed experimentally (Figs. 7b and 8b). The sensitivity of the calculations to ΔpK and ΔG_{chem} is seen in Fig. 7b. The two leftmost hatched curves are for a ΔpK value of 5.2, while the two right dashed curves are for $\Delta pK = 8.5$. In either set, the lower curve corresponds to $\Delta G_{\text{chem}} = 0$. Roughly speaking, the value of ΔpK controls the pH at which the upturn in adsorption occurs, and ΔG_{chem} controls the magnitude of adsorption density.

The Ni adsorption data could be matched reasonably well using a ΔpK value of 7, along with a chemical term of 7 KJ/mol. A different ΔpK value is perhaps justified for the Ni data since the results are from a different group (38) and a different type of silica was used. However, the ΔpK value of 8.5 needed to simulate the Ca data is not justified, since this data is from the same reference as the Co, Cr, and Fe data (1–3) and employed the same silica support. A different pretreatment, such as a high temperature calcination which can eliminate hydroxyl groups, was not mentioned in the paper (1) and the possibility of an impurity which can alter the isoelectric point and charge is highly unlikely. In fact, for both Ca and Ni the experimental adsorption data does more closely emulate the liquid-phase speciation of the first

hydrolysis products. The first hydrolysis products may indeed be adsorbed predominantly in these latter two cases, especially in the case of calcium. This interpretation can be rendered in the revised model only by adding a repulsive (positive) chemical interaction term to the +2 species, while adding an attractive term to the +1 species. A possibility is that the solvation free energy is a stronger function of radius than in the term currently employed. The radius of calcium (Table 3) is far larger than any other modeled in this set over silica.

The calcium results notwithstanding, the revised model brings into question the prevalent interpretation of the original double-layer theory and many triple-layer theories that univalent species adsorb preferentially to multivalent species over oxide surfaces. The revised model presents a simple, predominantly electrostatic picture of the adsorption process in which the surface species largely reflect the liquid-phase species.

The adsorption of Pd complexes onto alumina at pH values both above and below the PZC of alumina has been claimed to be predominantly electrostatic in nature (38). A comparison of the revised physical adsorption model to the much-cited results of Contescu and Vass (39) is shown in Fig. 9. The non-Nernstian two-site amphoteric model is applied to calculate the interfacial potential. The values of alumina pzc (7.8), ΔpK (4.62), and N_s ($0.68e14$ site/cm²) were used as reported. The maximum uptakes of the chloride

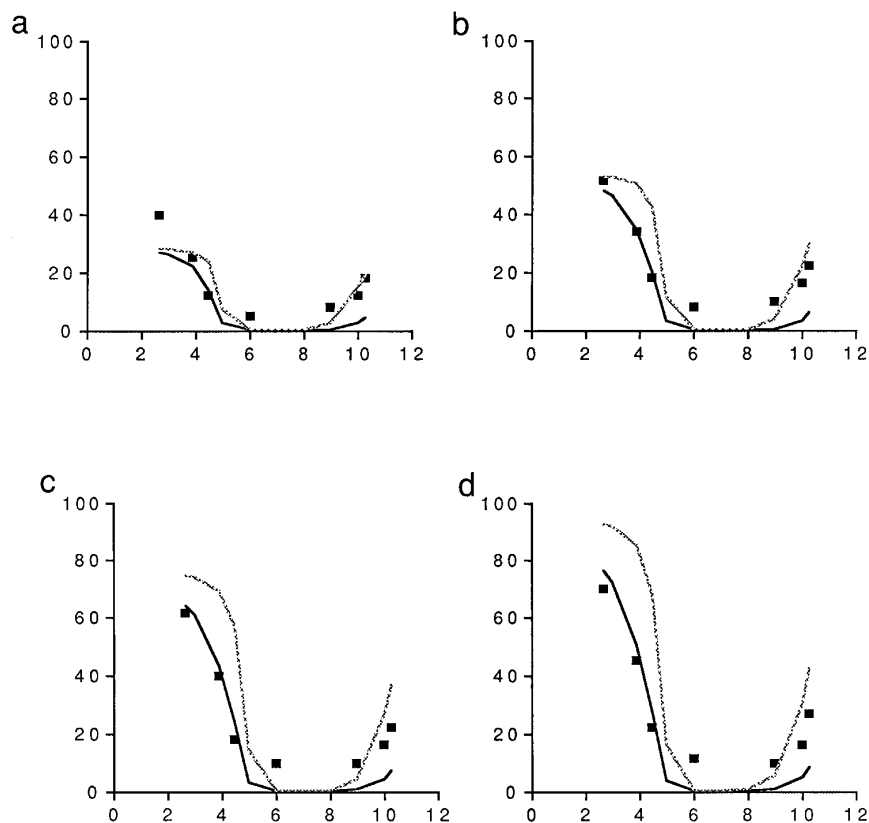


FIG. 9. Comparison of experimental (points) vs RPA model uptake of palladium on 3255 m²/liter of Al(III) oxide at 25°C with $\Delta pK = 4.62$ at initial metal concentration of (a) 0.5e-3 mol/liter, (b) 1.0e-3 mol/liter, (c) 1.5e-3 mol/liter, and (d) 2.0e-3 mol/liter at $N_s = 0.68e14$ sites/cm² (solid line) and $N_s = 8e14$ sites/cm² (dotted line).

and amine complexes were based on a close-packed monolayer of PdCl_4^{-2} retaining 1 hydration sheath (acidic pH), or on $\text{Pd}(\text{NH}_3)_4^{+2}$ retaining two hydration sheaths (basic pH), as found previously (27). The percentage of uptake versus pH is shown for four concentrations, 0.5, 1.0, 1.5, and 2.0 mmol Pd/liter. The calculations using the reported (and not adjusted) parameters are represented by the solid lines in Fig. 9. The fit is quite good in the low pH range but underestimates uptake in the high pH range, although the trend of the data is followed. If a more common value of $N_s = 8e14$ sites/cm² is used for the hydroxyl group density (calculations shown by hashed lines), the fit in the high pH region is excellent, while the low pH uptake is now overestimated somewhat. The relatively weak dependence of adsorption uptake on N_s can be seen from this figure; the two sets of results employ N_s values which differ by over an order of magnitude. An optimized value for N_s would fall roughly inbetween the two values shown.

At low pH, Pd exists primarily as palladium chloride, PdCl_4^{-2} , while at high pH, the main species is palladium tetraamine, $(\text{NH}_3)_4\text{Pd}^{+2}$ (39). This change in speciation is opposite to that of the surface charge, which is strong and positive at low pH, and strong and negative at high pH. The model predicts at either N_s value that these are in fact the

predominant adsorbed complexes. Thus the detailed simulation of Contescu and Vass' data with the current model supports the original claim of a primarily electrostatic adsorption mechanism.

James and Healy's model can also be applied to conditions where net electrostatic repulsion occurs, as in cation adsorption over positively charged goethite and chromia (5–7) surfaces (at pH values below the oxide pzc). A comparison of the original and revised models for representative results from Refs. (5–7) are shown in Fig. 10. Utilizing a ΔpK of 7 and estimating hydroxyl site density to be $N_s = 17e14$ sites/cm² (9, 33), good fits to all data sets are obtained with ΔG_{chem} values substantially lower than those employed in the original model. In these simulations, the ΔG_{chem} must be used to compensate the coulombic and solvation terms, which are now both repulsive. Values are lower for the RPA model since, first, the surface potentials and therefore the coulombic terms are smaller (see Fig. 1), and second, because the solvation terms are smaller. When a ΔpK value of 5 is used, ΔG_{chem} values are somewhat higher than those used for a ΔpK of 7 since the surface potential is now higher, but they are still below those of the original model. A comparison of individual ΔG values for the two models is given in Table 3. From this table it is also seen that the

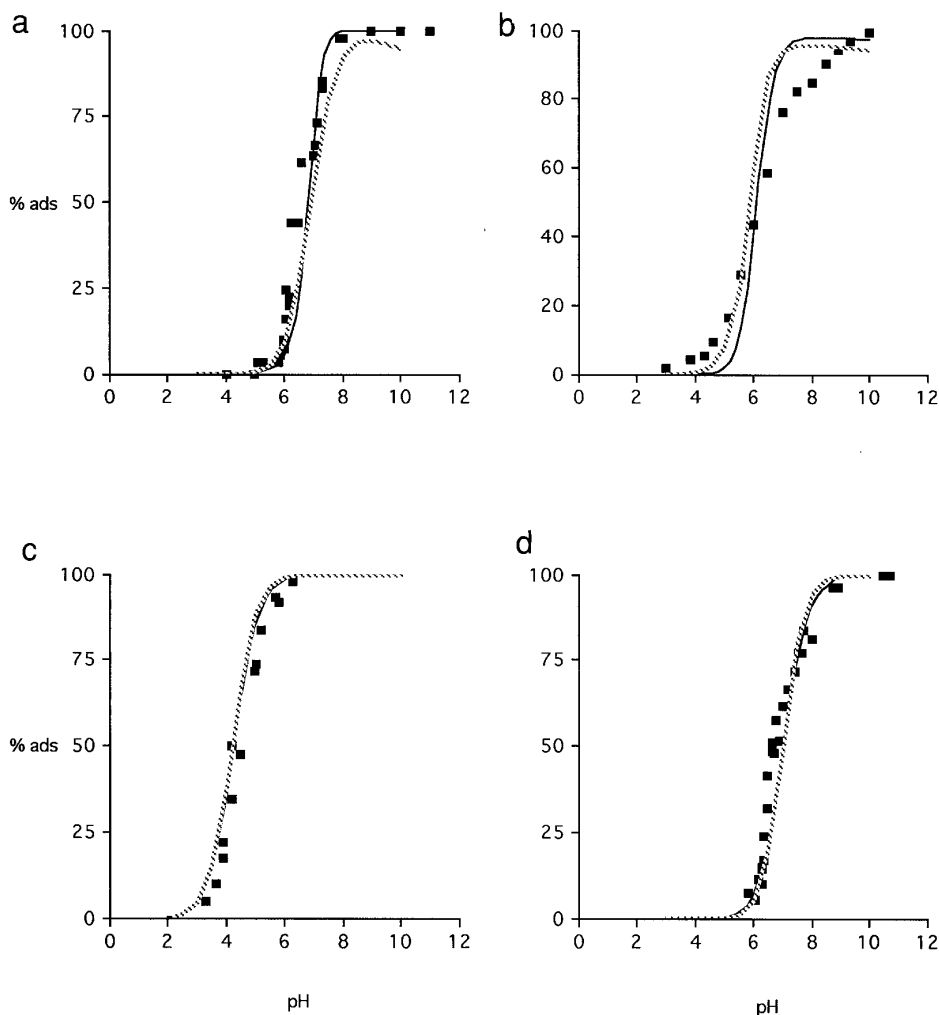


FIG. 10. Comparison of experimental (points) vs RPA model (line) uptake of (a) zinc ($r_{Zn} = 0.74 \text{ \AA}$) on goethite (Ref. (6), Fig. 5), (b) lead ($r_{Pb} = 0.74 \text{ \AA}$) on goethite (Ref. (7), Fig. 3), (c) chromium on goethite (Ref. (6), Fig. 3), (d) nickel on Cr(III) oxide (Ref. (6), Fig. 6).

+1 species (first hydrolysis products) and not the +2 metal ions are predicted by both models to be preferentially adsorbed since in both the sum of the coulombic and solvation free energies is smaller for the univalent species. (This sum is actually smallest for the zero-valent second hydrolysis products, but the concentrations of these species in the pH range of import is negligible.)

In the simulations of Fig. 10 the chemical terms of both double-layer models are greater than the sum of the coulombic and solvation energy terms (Table 3), and strictly speaking they should no longer be considered models of “physical adsorption.” The applicability of the RPA to other systems which exhibit predominantly “chemical adsorption” like those in Fig. 10 will be investigated. The RPA model is much simpler and contains fewer adjustable parameters than current triple-layer models, as well as the simplified double-layer models of Dzombak and Morel (11).

Current efforts are focused on utilizing the RPA model to describe adsorption as occurs in catalyst impregnation, that is, on a more scientific description of catalyst preparation. The model is being applied to noble metal complex adsorption onto oxides such as silica and alumina which are commonly used as catalyst supports. Preliminary results such as those in Fig. 9 indicate that good agreement to experiment can be attained without the use of the ΔG_{chem} term; adsorption in these cases may well be purely physical in nature.

APPENDIX: NOMENCLATURE

c	concentration of background electrolyte in the solution (mole/liter)
C_i	concentration of species i with valence z_i remaining in solution at equilibrium (mole/liter)

$C_{i,\text{in}}$	initial concentration of species i (i.e., before adsorption calculations) (mole/liter)	$10^{-12} \text{ J}^{-1} \text{ C}^2 \text{ m}^{-1}$	ϵ_p	dielectric constant of the metal oxide (4.3, Si; 14.2, Al; 14.2, Fe; 8.0, Cr)
$C_{i,\text{ads}}$	concentration loss of species i due to adsorption (mole/liter)		ϵ_1	dielectric constant of interfacial aqueous medium
e	charge of electron (1.60219×10^{-19} coul)		κ	inverse of the electric double layer length (m^{-1})
F	Faraday constant (96501.2 coul/mole)		Γ_i	adsorption density of species i (mole/ m^2)
$\Delta G_{\text{ads},i}$	change in total Gibbs free energy of adsorption of species i (J/mole)		Γ_{mi}	maximum adsorption density of species i (mole/ m^2)
$\Delta G_{\text{coul},i}$	change in coulombic free energy of adsorption of species i (J/mole)		Γ_{T}	total adsorption density (mole/ m^2)
$\Delta G_{\text{solv},i}$	change in solvation free energy of adsorption of species i (J/mole)		σ_0	surface charge density (coul/ cm^2)
$\Delta G_{\text{chem},i}$	change in chemical free energy of adsorption of species i (J/mole)		σ_d	diffuse layer charge density (coul/ cm^2)
H	concentration of protons in the solution (mole/liter)		$\psi_{x,i}$	potential at the hydration radius away from the oxide surface imposed on adsorbate molecules (volt)
H_s^+	concentration of surface protons		ψ_0	oxide surface potential (volt)
I	ionic strength (mole/liter)		θ	total surface coverage of the oxide by the metal species
k	Boltzmann's Constant ($1.38066 \times 10^{-23} \text{ J/K}$)		θ_i	fractional surface coverage of the oxide by the metal species i
K'_1, K'_2	surface ionization constants		$\Delta \text{p}K$	difference between $\text{p}K'_1$ and $\text{p}K'_2$
K_i	interfacial stability constant for species i , (liter/mole)			
m_{OX}	mass of the oxide (gm)			
N_0	Avogadro's number ($6.023 \times 10^{23} \text{ mole}^{-1}$)			
N_s	oxide surface site density (site/ cm^2)			
pH_{pzc}	pH at the point of zero charge			
$\text{p}K'_1, \text{p}K'_2$	negative log of surface ionization constants			
R	universal gas constant (8.314 J/mole K)			
r_i	radius of the adsorbate species (m)			
r_w	radius of water molecule (m)			
$[\text{SiOH}], [\text{SiO}]^-$	concentration of surface charged groups (mole/ cm^2) on SiO_2			
$[\text{AlOH}], [\text{AlO}]^-, [\text{AlOH}_2^+]$	concentration of surface charged groups (mole/ cm^2) on Al_2O_3			
S_{OX}	surface area of the metal oxide (m^2/gm)			
T	temperature (K)			
V_L	liquid volume (liter)			
Z	Valance of anion or cation of the symmetric supporting electrolyte (1 for 1:1 electrolytes)			
z_i	valance charge of adsorbate species			

Greek Characters

$\epsilon, \epsilon_{\text{bulk}}$	dielectric constant of the bulk aqueous medium (78.54) at room temperature
ϵ_0	dielectric constant of the free space (8.854188 \times

REFERENCES

- James, R. O., and Healy, T. W., *J. Colloid Interface Sci.* **40**, 42 (1972).
- James, R. O., and Healy, T. W., *J. Colloid Interface Sci.* **40**, 53 (1972).
- James, R. O., and Healy, T. W., *J. Colloid Interface Sci.* **40**, 65 (1972).
- MacNaughton, M. G., and James, R. O., *Soil Sci. Soc. Am. J.* **46**, 56 (1982).
- Crawford, R. J., Harding, I. H., and Mainwaring, D. E., *Langmuir* **9**, 3050 (1993).
- Crawford, R. J., Harding, I. H., and Mainwaring, D. E., *Langmuir* **9**, 3057 (1993).
- Rodda, D. P., Johnson, B. B., and Wells, J. D., *J. Colloid Interface Sci.* **161**, 57 (1993).
- Weise, G. R., James, R. O., and Healy, T. W., *Chem. Soc. London Faraday Discuss.* **51**, 302 (1971).
- Davis, J. A., and Leckie, J. O., *J. Colloid Interface Sci.* **67**, 90 (1978).
- Hayes, K. F., and Leckie, J. O., *J. Colloid Interface Sci.* **115**, 564 (1987).
- Dzombak, D. A., and Morel, F. M. M., "Surface Complexation Modeling: Hydrous Ferric Oxide." Wiley, New York, 1990.
- Ludwig, C., and Schindler, P. W., *J. Colloid Interface Sci.* **169**, 284 (1995).
- Ludwig, C., and Schindler, P. W., *J. Colloid Interface Sci.* **169**, 291 (1995).
- Zhang, Q., Xu, Z., and Finch, J. A., *J. Colloid Interface Sci.* **169**, 414 (1995).
- Zhang, Q., Xu, Z., and Finch, J. A., *J. Colloid Interface Sci.* **175**, 61 (1995).
- Lutzenkirchen, J., Magnico, P., and Behra, P., *J. Colloid Interface Sci.* **170**, 326 (1995).
- Katz, L. E., and Hayes, K. F., *J. Colloid Interface Sci.* **170**, 477 (1995).
- Katz, L. E., and Hayes, K. F., *J. Colloid Interface Sci.* **170**, 491 (1995).
- Tiffreau, C., Lutzenkirchen, J., and Behra, P., *J. Colloid Interface Sci.* **172**, 82 (1995).
- Yiacoumi, S., and Tien, C., *J. Colloid Interface Sci.* **175**, 333 (1995).
- Yiacoumi, S., and Tien, C., *J. Colloid Interface Sci.* **175**, 347 (1995).
- Sverjensky, D. A., *Nature* **364**, 776 (1993).
- Bontha, J. R., and Pintauro, P. N., *J. Phys. Chem.* **96**, 7778 (1992).
- Fuerstenau, D. W., and Osseo-Asare, K., *J. Colloid Interface Sci.* **118**, 524 (1987).

25. Healy, T. W., Yates, D. E., White, L. R., and Chan, D., *J. Electroanal. Chem.* **80**, 57 (1977).
26. Healy, T. W., and White, L. R., *Adv. Colloid Interface Sci.* **9**, 303 (1978).
27. Santhanam, N., Conforti, T. A., Spieker, W., and Regalbuto, J. R., *Catal. Today*, **21**, 141 (1994).
28. James, R. O., and Parks, G. A., *Surf. Colloid Sci.* **12**, 119 (1982).
29. Yates, D. E., Levine, S., and Healy, T. W., *Chem. Soc. Faraday Trans. I* **70**, 1807 (1974).
30. Sprycha, R., and Szczypa, J., *J. Colloid Interface Sci.* **102**, 288 (1984).
31. Noh, J. S., and Schwarz, J. A., *J. Colloid Interface Sci.* **139**, 139 (1990).
32. James, R. O., Davis, J. A., and Leckie, J. O., *J. Colloid Interface Sci.* **65**, 331 (1978).
33. Davis, J. A., James, R. O., and Leckie, J. O., *J. Colloid Interface Sci.* **63**, 480 (1978).
34. Park, J., and Regalbuto, J. R., *J. Colloid Interface Sci.* **175**, 239 (1995).
35. Sacher, E., and Laidler, K. J., "Modern Aspects of Electrochemistry" (J. O. Bockris and B. E. Conway, Eds.), No. 3. Butterworths, London, 1964.
36. Andersen, T. N., and Bockris, J. O., *Electrochem. Acta* **9**, 347 (1964).
37. James, R. O., Ph.D. dissertation, Stanford University, 1972.
38. Theis, T. L., and Richter, R. O., "Particulates in Water" (M. C. Kavanaugh and J. O. Leckie, Eds.), Advances in Chemistry Series No. 189, Chap. 4, p. 73. Am. Chem. Soc., Washington DC, 1980.
39. Contescu, Cr., and Vass, M. I., *Appl. Catal.* **33**, 259 (1987).